State-Space Modeling of Grid-Connected Power Converters Considering Power-Internal Voltage Characteristics

Peng, Qiao; Yang, Yongheng; Blaabjerg, Frede

Published in:
Proceedings of 2019 10th International Conference on Power Electronics and ECCE Asia (ICPE 2019 - ECCE Asia)

Publication date:
2019

Document Version
Accepted author manuscript, peer reviewed version

State-Space Modeling of Grid-Connected Power Converters Considering Power-Internal Voltage Characteristics

Qiao Peng, Yongheng Yang, and Frede Blaabjerg
Department of Energy Technology, Aalborg University, Aalborg 9220, Denmark
Email: qpe@et.aau.dk, yoy@et.aau.dk, fbl@et.aau.dk

***Abstract*—To analyze the stability of power electronics-dominated systems, this paper develops a state-space model of power converters including the DC-link voltage control, where the power-internal voltage (PIV) characteristics of the power converters are considered. The PIV concept comes from the inertia characteristic and swing equation of synchronous generators. It reflects the relationship between the output power and converter internal voltage, the converter response to grid disturbances, and finally, the impact of power converters on the grid stability. In the proposed model, the inputs are the outer controller references and the converter output power, i.e., the power at the point of common coupling (PCC). The output of the model is the internal voltage that determines the grid power distribution, including the power at the PCC. The power will be fed back to the converters as an input, and thinks the closed-loop model of the converter-based system is obtained. Importantly, the parameters of the proposed model are independent of the power grid, but related to the converter operation points and parameters. This makes the model more general and can be employed to analyze multiple converter-based systems. Furthermore, a case study is conducted in this paper to demonstrate the model and the stability analysis.**

***Index Terms*—Grid-connected power converter; modeling; internal voltage; external characteristics; power angle stability; power electronics-based power systems**

I. Introduction

The fast development of renewable energy has made the conventional power systems complicated with more power electronics, toward power electronics-dominated systems. Power electronic converters with fast dynamics and sophisticated controllers make the entire system to operate more flexibly and efficiently. On the other hand, challenging issues are arising in this case [1], [2]. One of the challenges is that the power electronic converters are controlled by various control strategies, which are difficult to be synthesized and thereby operate in harmony. In this context, the stability analysis of the systems with multiple converters could be over-complicated if all the converters are modeled precisely. Additionally, an effective way to evaluate the impact of power electronics on the conventional grid is of high concern in order to further increase the renewable energy penetration [3].

It thus calls for a universal assessment model that can be applied to converters with different control strategies, and it should also be simplified properly for the potential system expansion, as illustrated in [4]. Moreover, the concept of virtual inertia has been presented as an important and effective tool for the stability enhancement of power electronics-dominated systems [5]. Inertia is one of the inherent characteristics of the conventional synchronous generator (SG). It determines the power angle stability, i.e., the voltage phase angle difference between the internal voltage and terminal voltage of the SG, and further the active power and frequency stability of the entire system [6]. Accordingly, the power converter with a novel control strategy was developed as a virtual synchronous generator (VSG) [7], [8]. However, the operation of VSGs is supported by large-capacity energy storage systems (ESSs), which is not specially economical and practical. For the widespread converters without ESSs, the power-internal voltage (PIV) characteristics, which are directly related to the converter virtual inertia, are difficult to explore.

Certain attempts have been made into the inertia characteristics of converters without ESSs. For instance, the inertia can be alternatively generated from the mechanical rotor of wind turbines [9], photovoltaic systems [10], and DC-link capacitors, which are generally used in grid-connected converters for the DC-link voltage stability [11], [12]. The exploration of inertia emulating by the DC-link capacitor is practically viable, as it enables flexible frequency support from all power converters, especially in small-scale and relatively weak grids. Moreover, the outcomes would be general and representative, and it can be applied to the converters with more complicated control strategies. In this case, minor modifications may be necessary. For example, a state space model of the power converter disclosing the dynamics of the DC-link voltage considering the phase locked-loop (PLL) impact and AC voltage controller is presented in [13], but the theory has not been concluded systematically yet. The PIV characteristics are clearly demonstrated in [14], but the model is transfer function-based, which is not specifically applicable in multi-converter-based systems.

To shed light on the inertia of grid-connected converters, a state space model considering the PIV characteristics is developed in this paper. It is exemplified in the DC-link voltage-controlled converters for universal applications. The aim of the model is to to reveal the relationship between the output power and internal voltage of the power converter

This work was supported by THE VELUX FOUNDATIONS under the VILLUM Investigator Grant – REPEPS (Award Ref. No.: 00016591).

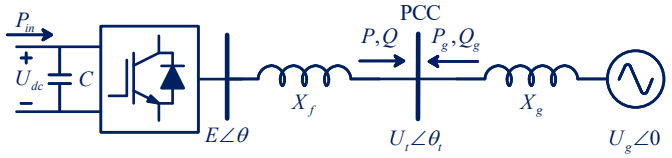

Fig. 1. Grid-feeding power converter-based AC grid, where $E\angle\theta$ and $U_t\angle\theta_t$ are the internal voltage and terminal voltage of the power converter, respectively, $U_g\angle 0$ is the voltage of the AC grid bus as the reference, C is the DC-link capacitor and U_{dc} is the DC-link voltage, X_f and X_g are the equivalent reactance of the output filter and the grid, respectively, P, Q and P_g, Q_g are the output powers from the power converter and the grid, and P_{in} is the input active power from DC sources.

emphatically. More importantly, the parameters in the model are all based on converter parameters and its operation points, being independent of the grid parameters, which makes it more practical and flexible for the application in multiple converter-based systems. A case study is presented, where simulations are performed to validate the model and the analysis.

II. Grid-Connected Converter and PIV Characteristics

In multi-SG-based systems, i.e., the conventional AC grids with less power electronics, the power angle stability and voltage stability are the two most important issues. The power angle, determined by the inertia of SGs, rules the active power distribution, and hence, the frequency stability of the systems. Inspired by this, the concept of inertia can be applied in the stability analysis of power electronics-based systems, where the power converters play the roles of SGs in conventional AC grids.

For power converters without physical rotors, the inertia can be emulated by the electrical energy transferring in energy storage devices, such as batteries and DC-link capacitors. The inertia generated by electrical energy is called virtual inertia. For a grid-connected converter as shown in Fig. 1, its virtual inertia characteristic can be represented by the relationship between the output power and the internal voltage, as indicated by P, Q and $E\angle\theta$ in Fig. 1 [15]. It is worth mentioning that the model will not include the grid parameters (e.g., X_g in Fig. 1), which makes it more friendly for the analysis of multiple converters-based systems.

For the dual-loop-controlled converters, the virtual inertia can be provided directly by charging and discharging the DC-link capacitor, if a DC-link voltage controller is adopted. Subsequently, a PIV characteristics-considered model can be obtained. However, when the active power control is applied, charging or discharging the DC-link capacitor cannot be controlled directly. Thus, the converters need supplementary energy sources, such as energy storage systems (ESSs), photovoltaic (PV) systems, or wind farms to provide the virtual inertia, and related additional control strategies are required. The PIV-considered model will be more complicated with additional devices corresponding to various supplementary energy sources. For simplicity, the DC-link voltage control and terminal voltage control are applied in this paper. When

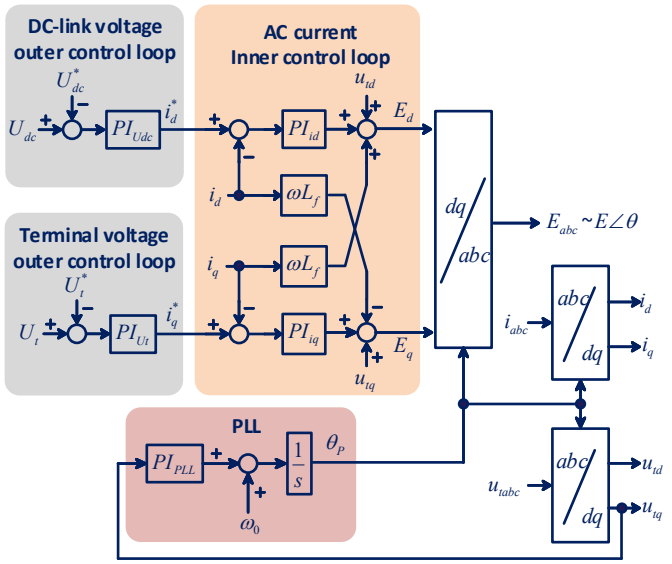

Fig. 2. Diagram of dual-loop control system in a grid-connected converter, where i is the AC current flowing through the filter, L_f is the filter inductor, θ_P is the output voltage phase of the PLL, the superscript "$*$" denotes the reference value, and the subscripts (d and q) represent the corresponding dq components based on the PLL output voltage phase.

the converter adopts other outer controllers such as active power controller, additional control loops are needed to emulate virtual inertia, and the model should be modified and improved. However, the concepts of virtual inertia and PIV characteristic are still available, and the entire system stability can be analyzed by assembling the inertia of all converters [14].

III. State Space Modeling of Grid-Connected Converters

The state space modeling of grid-connected converters reflecting their PIV characteristics will be illustrated in this section. The dual-loop vector control strategy is applied in this paper, where the DC-link voltage controller and terminal voltage controller are the outer controllers, as shown in Fig. 2. Certain assumptions should be made for simplicity:

1) The dynamics of the current control loops are neglected, i.e., it is assumed that the AC currents can immediately follow the reference currents;

2) The DC source is considered ideal, and the fluctuation of the converter input power from the DC side is ignored, i.e., $\Delta P_{in} = 0$;

3) The interaction of the active and reactive power in the control is ignored.

A. Voltage Phase Angle Relationship

The relationship of phase angles in the converter control system should be introduced firstly. Fig. 3 shows the voltage phase angles in steady state and after small disturbances, denoted in blue and red, respectively. As shown in Fig. 3, in steady state, the terminal voltage is typically aligned with the d-axis, which is determined by the PLL. When there is a

disturbance, the tracking error of the terminal voltage phase will be introduced in the PLL, and then makes the d-axis shift from the original voltage $\boldsymbol{u}_t$, as marked by the red sector in Fig. 3. The deviation may consequently affect the stability of the power converter and the AC grid. The voltage phase of the converter internal voltage can be derived as

$$\Delta\theta = (\theta_E^{P\prime} + \theta_P') - (\theta_{E0}^P + \theta_{P0}) = \Delta\theta_E^P + \Delta\theta_P \quad (1)$$

where θ, θ_P and θ_E^P are the internal voltage phase angle, PLL output phase angle and the difference between these two phase angles. The subscript "0" denotes the initial value in steady state, and the superscript "$\prime$" denotes the value after the disturbances.

B. Power Exchange between Internal and Terminal Voltages

The voltage drop on the filter inductor can be given as

$$\boldsymbol{e} = \boldsymbol{U}_t + jX_f\boldsymbol{i} \quad (2)$$

where $\boldsymbol{e}$, $\boldsymbol{U_t}$ and $\boldsymbol{i}$ are the internal voltage, terminal voltage and AC current at the point of common coupling (PCC), X_f is the filter reactance. Decomposing (2) into the dq-frame and neglecting the steady-state voltage phase angle difference between E_0 and U_{t0} result in

$$\Delta E = \Delta U_t - X_f\Delta i_q \quad (3)$$

$$\Delta\theta_E^P = \frac{X_f}{E_0}\Delta i_d + \frac{U_{t0}}{E_0}\Delta\theta_t^P \quad (4)$$

The active and reactive power flow from the internal voltage to the terminal voltage are given as

$$P = \frac{EU_t sin(\theta - \theta_t)}{X_f} \quad (5)$$

$$Q = \frac{E^2 - EU_t cos(\theta - \theta_t)}{X_f} \quad (6)$$

Linearizing (5)-(6) yields

$$\Delta\theta = \Delta\theta_t + \frac{X_f}{E_0U_{t0}}\Delta P \quad (7)$$

$$\Delta E = \frac{E_0}{2E_0 - U_{t0}}\Delta U_t + \frac{X_f}{2E_0 - U_{t0}}\Delta Q \quad (8)$$

According to Eqs. (3)-(4) and (7)-(8), it can be obtained that

$$\Delta\theta_t^P = \frac{X_f}{E_0 - U_{t0}}\Delta i_d - \frac{X_f}{U_{t0}(E_0 - U_{t0})}\Delta P \quad (9)$$

$$\Delta\theta_E^P = \frac{X_f}{E_0 - U_{t0}}\Delta i_d - \frac{X_f}{E_0(E_0 - U_{t0})}\Delta P \quad (10)$$

$$\Delta U_t = \frac{(2E_0 - U_{t0})X_f}{E_0 - U_{t0}}\Delta i_q + \frac{X_f}{U_{t0}(E_0 - U_{t0})}\Delta Q \quad (11)$$

$$\Delta E = \frac{E_0X_f}{E_0 - U_{t0}}\Delta i_q + \frac{X_f}{U_{t0}(E_0 - U_{t0})}\Delta Q \quad (12)$$

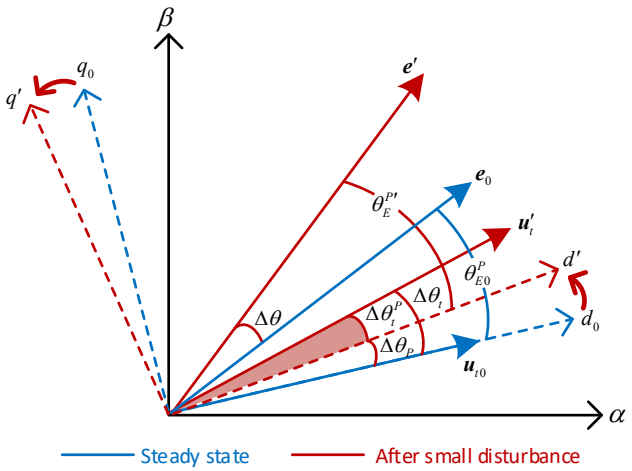

Fig. 3. Voltage phase angle relationship in the control system of power converters, where θ_E^P is the difference between the internal voltage phase and PLL output voltage phase, θ_t^P is the difference between the terminal voltage phase and PLL output voltage phase, the subscript "0" denotes the initial value in steady state, and the superscript "$\prime$" denotes the value after disturbances.

C. Outer Control Loops

The outer-loop controllers are designed to regulate the DC-link voltage controller and the terminal voltage, i.e., the voltage amplitude at the PCC. The deviation of the converter output active power will affect the charging or discharging states of the DC-link capacitor. From Fig. 1, it can be found that

$$\frac{d}{dt}\Delta U_{dc} = -\frac{1}{CU_{dc0}}\Delta P \quad (13)$$

As the dynamics of the inner current controller are neglected, they can be linearized as

$$\Delta i_d = \Delta\varphi_{dc} + k_{pdc}\Delta U_{dc} - k_{pdc}\Delta U_{dc}^* \quad (14)$$

$$\Delta i_q = \Delta\varphi_t + k_{pt}\Delta U_t - k_{pt}\Delta U_t^* \quad (15)$$

where k_{pdc} and k_{pt} are the proportional coefficients, k_{idc} and k_{it} are the integral coefficients of the PI controllers for the DC-link voltage controller and the terminal voltage controller. In addition, φ_{dc} and φ_t are defined as

$$\frac{d}{dt}\Delta\varphi_{dc} = k_{idc}\Delta U_{dc} - k_{idc}\Delta U_{dc}^* \quad (16)$$

$$\frac{d}{dt}\Delta\varphi_t = k_{it}\Delta U_t - k_{it}\Delta U_t^* \quad (17)$$

D. Phase-Locked Loop

The PLL applied in this paper is the synchronous reference frame phase-locked loop (SRF-PLL), which tracks the grid voltage phase angle by controlling the q-axis component of the voltage to zero at the PCC. The linearized model of the SRF-PLL is given as

$$\frac{d}{dt}\Delta\theta_P = \Delta\varphi_{pll} + k_{ppll}\Delta\theta_t^P \quad (18)$$

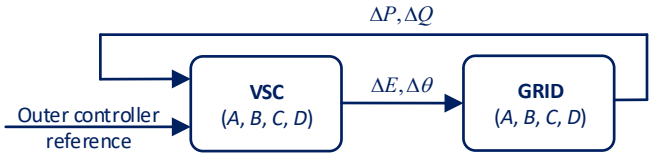

Fig. 4. Closed-loop model of the grid-connected converter considering the PIV characteristic, where A, B, C, D are the state matrices of the state space models.

in which k_{ppll} is the proportional coefficient of the PI controller in the PLL, and φ_{pll} is defined as

$$\frac{d}{dt}\Delta\varphi_{pll} = k_{ipll}\Delta\theta_t^P \tag{19}$$

where k_{ipll} is the integral coefficient of the PI controller in the PLL.

According to all the proposed modular models discussed in the above, the open-loop model of the grid-connected converter without feedback from the grid can be obtained as

$$\frac{d}{dt}\Delta\boldsymbol{x}_{con} = \boldsymbol{A}_{con}\Delta\boldsymbol{x}_{con} + \boldsymbol{B}^*_{con}\Delta\boldsymbol{U}^* + \boldsymbol{B}^g_{con}\Delta\boldsymbol{PQ} \tag{20}$$

$$\Delta\boldsymbol{y}_{con} = \boldsymbol{C}_{con}\Delta\boldsymbol{X}_{con} + \boldsymbol{D}^*_{con}\Delta\boldsymbol{U}^* + \boldsymbol{D}^g_{con}\Delta\boldsymbol{PQ} \tag{21}$$

with

$$\Delta\boldsymbol{x}_{con} = \begin{bmatrix}\Delta\varphi_{dc} & \Delta\varphi_{ac} & \Delta\varphi_{pll} & \Delta\theta_P & \Delta U_{dc}\end{bmatrix}^{-1}$$
$$\Delta\boldsymbol{U}^* = \begin{bmatrix}\Delta U^*_{dc} & \Delta U^*_t\end{bmatrix}^{-1}$$
$$\Delta\boldsymbol{PQ} = \begin{bmatrix}\Delta P & \Delta Q\end{bmatrix}^{-1}$$
$$\Delta\boldsymbol{y}_{con} = \begin{bmatrix}\Delta\theta & \Delta E\end{bmatrix}^{-1}$$

and the state matrices as given in Eqs. (22)-(26). In the power converter model shown in (20) and (21), one of the input vectors is the power at the PCC, and the output is the internal voltage of the power converter. It is easy to obtain the representation of the PIV characteristics as a transfer function transformed directly from the proposed state space model, as depicted in [14].

As mentioned, one of the advantages of the proposed model is that there is no grid parameter in the converter model, and it can connect to the grid easily in order to obtain the closed-loop model of the whole system. For the system shown in Fig. 1, the power exchange between the internal voltage and AC grid bus voltage is given as

$$P = \frac{EU_g sin\theta}{X_f + X_g} \tag{27}$$

$$Q = \frac{E^2 - EU_g cos\theta}{X_f + X_g} \tag{28}$$

which can be linearized without considering the coupling of the active power and reactive power as

$$\Delta\boldsymbol{PQ} = \boldsymbol{FB}\Delta\boldsymbol{y}_{con} \tag{29}$$

where $\boldsymbol{FB}$ is given in (30).

TABLE I
SIMULATION SYSTEM PARAMETERS

Parameters	Values
Rated power	20 kW
Rated DC voltage	780 V
Rated AC voltage	400 V
DC-link capacitor	10 mF
Converter inductance	2.53 mH
Equivalent grid inductance	2.53 mH
Fundamental frequency	50 Hz
(k_{pdc}, k_{idc})	(0.5, 50)
(k_{pt}, k_{it})	(0.5, 50)
(k_{ppll}, k_{ipll})	(50, 10000)

From (20), (21) and (29), the closed-loop model of the grid-connected converter considering the PIV characteristic can be obtained as shown in Fig. 4, and it can be given as

$$\frac{d}{dt}\Delta\boldsymbol{x}_{con} = \boldsymbol{A}_{grid}\Delta\boldsymbol{x}_{con} + \boldsymbol{B}_{grid}\Delta\boldsymbol{U}^* \tag{31}$$

$$\Delta\boldsymbol{y}_{con} = \boldsymbol{C}_{grid}\Delta\boldsymbol{X}_{con} + \boldsymbol{D}_{grid}\Delta\boldsymbol{U}^* \tag{32}$$

with

$$\boldsymbol{A}_{grid} = \boldsymbol{A}_{con} + \boldsymbol{B}^g_{con}(\boldsymbol{FB}^{-1} - \boldsymbol{D}^g_{con})^{-1}\boldsymbol{C}_{con}$$
$$\boldsymbol{B}_{grid} = \boldsymbol{B}^*_{con} + \boldsymbol{B}^g_{con}(\boldsymbol{FB}^{-1} - \boldsymbol{D}^g_{con})^{-1}\boldsymbol{D}^*_{con}$$
$$\boldsymbol{C}_{grid} = \boldsymbol{C}_{con} + \boldsymbol{D}^g_{con}(\boldsymbol{FB}^{-1} - \boldsymbol{D}^g_{con})^{-1}\boldsymbol{C}_{con}$$
$$\boldsymbol{D}_{grid} = \boldsymbol{D}^*_{con} + \boldsymbol{D}^g_{con}(\boldsymbol{FB}^{-1} - \boldsymbol{D}^g_{con})^{-1}\boldsymbol{D}^*_{con}$$

being the proposed model with the consideration of the PIV characteristics.

IV. Model Validation and Stability Analysis

To validate the proposed model and to demonstrate its application in stability analysis, a case study is presented in this section. A converter connected to the grid as shown in Fig. 1 is simulated, where the synchronous reference frame-PLL (SRF-PLL) is applied, and the basic parameters are given in Table I.

A. Model Validation

At the first, the model is validated by the detailed simulation model in PSCAD/EMTDC. The DC-link voltage reference increases 10% at t = 2 s. The responses of the DC-link voltage U_{dc} and the d-component of AC current i_d are given in Fig. 5, where the orange curve and the blue curve correspond to the time-domain simulation and the system with the proposed model, respectively. It can be seen that the two curves are matching well, including the overshoot and damping speed. Thus, it can be concluded that the model proposed in this paper is effective.

B. Eigenvalue Analysis

Based on the validated model, stability analysis can be done as following. As the state matrices of the system are obtained directly, the system eigenvalues can be calculated and analyzed. Keeping other parameters unchanged except for the

$$\boldsymbol{A}_{con}=\begin{bmatrix} 0 & 0 & 0 & 0 & k_{idc} \\ 0 & k_{it}K_{Ut}(2E_0-U_{t0})X_f & 0 & 0 & 0 \\ k_{ipll}X_f/(E_0-U_{t0}) & 0 & 0 & 0 & k_{ipll}X_fK_{pdc}/(E_0-U_{t0}) \\ k_{ppll}X_f/(E_0-U_{t0}) & 0 & 1 & 0 & k_{ppll}X_fK_{pdc}/(E_0-U_{t0}) \\ 0 & 0 & 0 & 0 & 0 \end{bmatrix} \tag{22}$$

$$\boldsymbol{B}^*_{con}=\begin{bmatrix} -k_{idc} & 0 \\ 0 & -[k_{it}K_{Ut}(2E_0-U_{t0})X_fk_{pt}+k_{it}] \\ -k_{ipll}X_fk_{pdc}/(E_0-Ut0) & 0 \\ -k_{ppll}X_fk_{pdc}/(E_0-Ut0) & 0 \\ 0 & 0 \end{bmatrix},$$

$$\boldsymbol{B}^g_{con}=\begin{bmatrix} 0 & 0 \\ 0 & k_{it}K_{Ut}X_f \\ -k_{ipll}X_f/[U_{t0}(E_0-U_{t0})] & 0 \\ -k_{ppll}X_f/[U_{t0}(E_0-U_{t0})] & 0 \\ -1/(CU_{dc0}) & 0 \end{bmatrix} \tag{23}$$

$$\boldsymbol{C}_{con}=\begin{bmatrix} X_f/(E_0-U_{t0}) & 0 & 0 & 1 & X_fk_{pdc}/(E_0-U_{t0}) \\ 0 & E_0K_{Ut}X_f & 0 & 0 & 0 \end{bmatrix} \tag{24}$$

$$\boldsymbol{D}^*_{con}=\begin{bmatrix} -X_fk_{pdc}/(E_0-U_{t0}) & 0 \\ 0 & -E_0K_{Ut}X_fk_{pt} \end{bmatrix},$$

$$\boldsymbol{D}^g_{con}=\begin{bmatrix} -X_f/[E_0(E_0-U_{t0})] & 0 \\ 0 & (E_0K_{Ut}X_f+X_f)/(2E_0-U_{t0}) \end{bmatrix} \tag{25}$$

$$K_{Ut}=1/[(E_0-U_{t0})-(2E_0-U_{t0})X_fk_{pt}] \tag{26}$$

$$\boldsymbol{FB}=\begin{bmatrix} E_0U_{g0}cos\theta_0/(X_f+X_g) & 0 \\ 0 & (2E_0-U_{g0}cos\theta_0)/(X_f+X_g) \end{bmatrix} \tag{30}$$

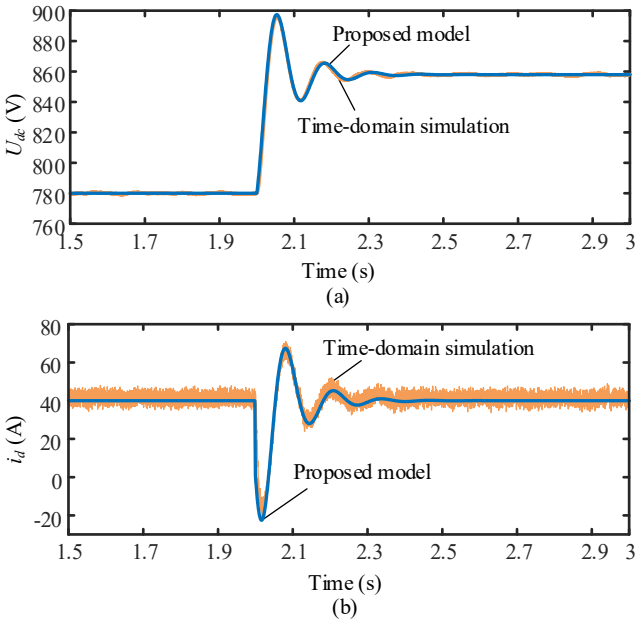

Fig. 5. Performance of the proposed model when the DC-link voltage reference increases by 10%: (a) DC-link voltage and (b) d-component of AC current.

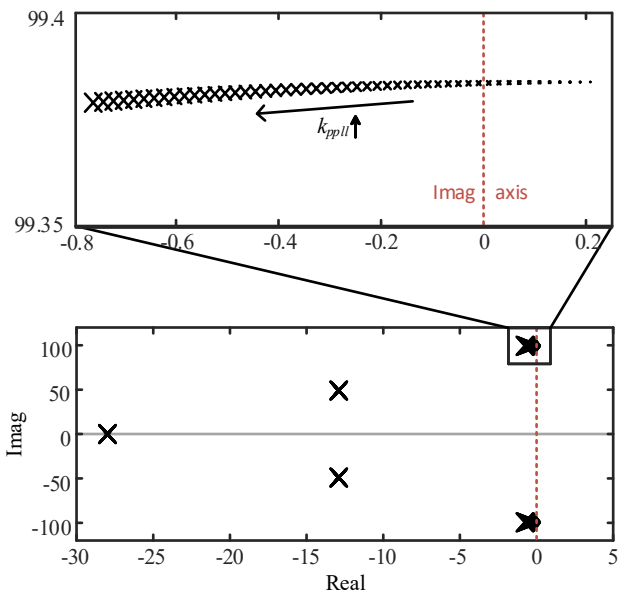

Fig. 6. Closed-loop eigenvalues of A_{grid} with increasing k_{ppll} for the VSC under study.

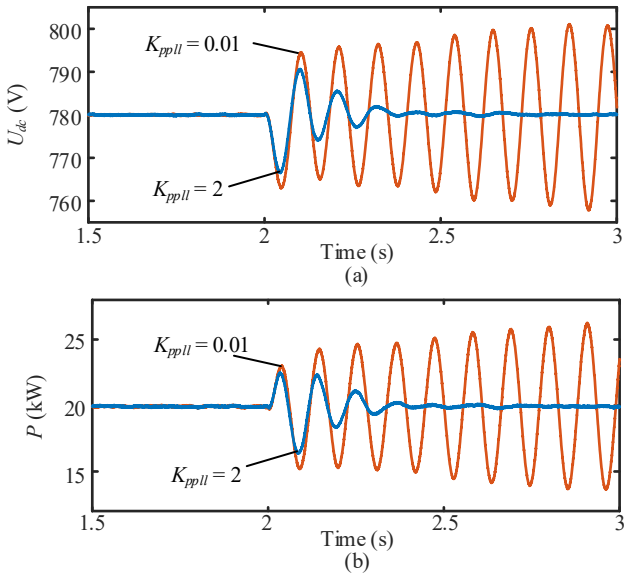

Fig. 7. Simulation results of the system under a disturbance with k_{ppll} = 0.01 and 2: (a) DC-link voltage and (b) d-component of AC current.

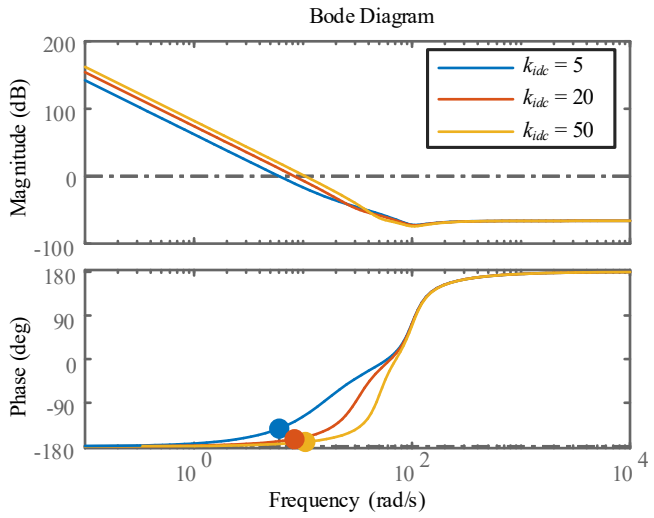

Fig. 8. Bode diagrams of the open-loop system with k_{idc} = 5, 20, and 50.

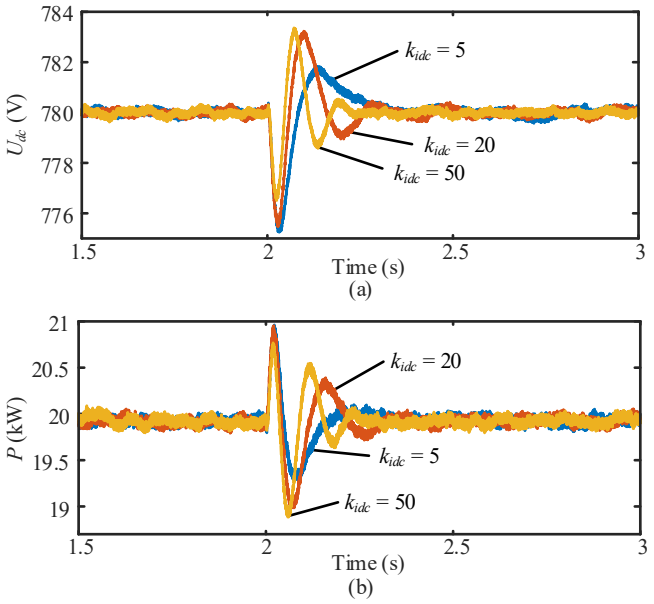

Fig. 9. Simulation results of the system under a disturbance with k_{idc} = 5, 20, and 50: (a) DC-link voltage and (b) d-component of AC current.

proportional gain of the PI controller in the PLL k_{ppll}, which is increased from 0.01 to 2, the eigenvalues of the closed-loop model, i.e., the eigenvalues of $\boldsymbol{A}_{grid}$ can be obtained, as shown in Fig. 6. It can be seen from Fig. 6 that when k_{ppll} increases from 0.01 to 2, the dominant eigenvalues will cross the imaginary axis (the red dot line). The result demonstrates that when k_{ppll} is too small, the system is unstable due to the lack of damping, but when k_{ppll} increases to a larger value, the system becomes stable with the eigenvalues moving to the left half-plane region.

To further validate the eigenvalue analysis results, a case study is carried out on the test system. At t = 2 s, a disturbance is imposed, where the phase angle of the AC grid bus voltage increases by 45°. The DC-link voltage and converter output active power responding to k_{ppll} = 0.01 and 2 are given in Fig. 7. It is observed in Fig. 7 that when k_{ppll} = 0.01, the system is poorly damped and oscillates severely. When k_{ppll} = 2, the oscillation can be damped effectively, and the system becomes stable. The simulation results are in close agreement with the eigenvalue analysis, which confirms the effectiveness of the proposed model in terms of stability analysis.

C. Bode Diagram Analysis

The Bode diagram is another important way to assess the system stability. The impact of the DC-link voltage controller on the system stability will be analyzed by the Bode diagram in this section. In this case, the system parameters are the same as given in Table I, but the integral gain of the PI controller for the DC-link voltage has been changed, i.e., k_{idc} = 5, 20, and 50. The Bode diagrams of the open-loop model from the input ΔP to the output $\Delta\theta$ are obtained, as shown in Fig. 8. It can be seen that when k_{idc} increases, the open-loop system phase margin will become smaller, i.e., the system stability is attenuated. To validate the analysis, a case study is performed on the simulation model. At t = 2 s, a disturbance is imposed, where the phase angle of the AC grid bus voltage increases by 45°. The DC-link voltage and converter output active power response with k_{idc} = 5, 20, and 50 are given in Fig. 9. It can be seen from Fig. 9 that although the DC-link voltage suffers a bit larger overshoot under disturbance with smaller k_{ppll}, the oscillation can be damped to a large extent in this case. As for the converter output active power, it is more obvious that the oscillation under disturbance can be suppressed faster with smaller k_{ppll}. To sum up, a smaller k_{ppll} can promise a better damping capability of a power converter, i.e., the system is more stable with a smaller k_{idc}, which confirms the Bode

diagram analysis.

V. Conclusion

A state space model of grid-connected converters considering the power-internal voltage characteristics is proposed in this paper. Referring to the swing equations of the synchronous generator, the developed model provides reduced but necessary information to the grid, i.e., the amplitude and phase angle of the internal voltage, which contribute to the grid power distribution. The power distribution of the grid will feedback to the converter as inputs, and the closed-loop model of the power converter-based systems can be obtained, based on which the system overall stability can be analyzed in a convenient way. One of the advantages of the proposed model is that the parameters are solely dependent on the converter parameters and their operation points, which makes it more practical than other models and it can be applied in large-scale and multi-converter-based systems. Several case studies have been performed, which validates the model and the stability analysis. Moreover, it has been revealed that the proposed model is accurate in the stability analysis of power converters. Based on the proposed model, the control parameters of converters can be designed to satisfy the DC-link voltage requirement or other stability demands.

References

[1] F. Blaabjerg, Y. Yang, D. Yang, and X. Wang, "Distributed Power-Generation Systems and Protection," *Proc. IEEE*, vol. 105, no. 7, pp. 1311–1331, Jul. 2017.

[2] B. K. Bose, "Global Energy Scenario and Impact of Power Electronics in 21st Century," *IEEE Trans. Ind. Electron.*, vol. 60, no. 7, pp. 2638–2651, Jul. 2013.

[3] Q. Peng, Y. Yang, H. Wang, and F. Blaabjerg, "On Power Electronized Power Systems: Challenges and Solutions," in *Proc. IEEE Ind. Appl. Soc. Annual Meeting*, Portland, OR, USA, Sep. 2018, pp. 1–9.

[4] H. Yuan, X. Yuan, and J. Hu, "Modeling of Grid-Connected VSCs for Power System Small-Signal Stability Analysis in DC-Link Voltage Control Timescale," *IEEE Trans. Power Syst.*, vol. 32, no. 5, pp. 3981–3991, Sep. 2017.

[5] J. Fang, H. Li, Y. Tang, and F. Blaabjerg, "On the Inertia of Future More-Electronics Power Systems," *IEEE J. Emerg. Sel. Top. Power Electron.*, early access, doi: 10.1109/JESTPE.2018.2877766.

[6] P. Kundur, N. J. Balu, and M. G. Lauby, *Power System Stability and Control*. New York: McGraw-hill, 1994.

[7] Q.-C. Zhong and G. Weiss, "Synchronverters: Inverters That Mimic Synchronous Generators," *IEEE Trans. Ind. Electron.*, vol. 58, no. 4, pp. 1259–1267, Apr. 2011.

[8] J. Alipoor, Y. Miura, and T. Ise, "Power System Stabilization Using Virtual Synchronous Generator With Alternating Moment of Inertia," *IEEE J. Emerg. Sel. Top. Power Electron.*, vol. 3, no. 2, pp. 451–458, Jun. 2015.

[9] J. Ying, X. Yuan, J. Hu, and W. He, "Impact of Inertia Control of DFIG-Based WT on Electromechanical Oscillation Damping of SG," *IEEE Trans. Power Syst.*, vol. 33, no. 3, pp. 3450–3459, May 2018.

[10] S. I. Nanou, A. G. Papakonstantinou, and S. A. Papathanassiou, "A generic model of two-stage grid-connected PV systems with primary frequency response and inertia emulation," *Electr. Power Syst. Res.*, vol. 127, pp. 186–196, Oct. 2015.

[11] J. Fang, H. Li, Y. Tang, and F. Blaabjerg, "Distributed Power System Virtual Inertia Implemented by Grid-Connected Power Converters," *IEEE Trans. Power Electron.*, vol. 33, no. 10, pp. 8488–8499, Oct. 2018.

[12] J. Fang, P. Lin, H. Li, Y. Yang, and Y. Tang, "An Improved Virtual Inertia Control for Three-Phase Voltage Source Converters Connected to a Weak Grid," *IEEE Trans. Power Electron.*, early access, doi: 10.1109/TPEL.2018.2885513.

[13] Y. Huang, X. Yuan, J. Hu, and P. Zhou, "Modeling of VSC Connected to Weak Grid for Stability Analysis of DC-Link Voltage Control," *IEEE J. Emerg. Sel. Top. Power Electron.*, vol. 3, no. 4, pp. 1193–1204, Dec. 2015.

[14] Q. Peng, J. Fang, Y. Yang, and F. Blaabjerg, "A Universal Model for Grid-Connected Converters Reflecting Power-Internal Voltage Characteristics," in *Proc. of 2018 IEEE 4th Southern Power Electron. Conf. (SPEC)*, Dec. 2018, pp. 1–7.

[15] J. Hu, J. Zhu, and M. Wan, "Modeling and Analysis of Modular Multilevel Converter in DC Voltage Control Timescale," *IEEE Trans. Ind. Electron.*, vol. 66, no. 8, pp. 6449–6459, Aug. 2019.